

# CLUES IN BAILEY DIAGRAMS INDICATE THAT THE HORIZONTAL BRANCH EVOLUTIONARY EFFECT IS THE DIRECT REASON FOR OOSTERHOFF PHENOMENON

LI, L.-J.,<sup>1</sup> QIAN, S.-B.,<sup>1,2,3</sup> ZHU, L.-Y.,<sup>1,4</sup> SHI, X.-D.,<sup>1</sup> AND LIAO, W.-P.<sup>1,4</sup>

<sup>1</sup>Yunnan Observatories, Chinese Academy of Sciences, P.O. Box 110, Kunming, 650216, People's Republic China

<sup>2</sup>Department of Astronomy, School of Physics and Astronomy, Yunnan University, Kunming 650091, People's Republic of China

<sup>3</sup>Key Laboratory of Astroparticle Physics of Yunnan Province, Yunnan University, Kunming 650091, People's Republic of China

<sup>4</sup>University of Chinese Academy of Sciences, No.1 Yanqihu East Rd, Huairou District, Beijing, 101408, People's Republic China

Submitted to ApJ

## ABSTRACT

Noticing the potential relationship between the pulsation amplitude of fundamental mode RR Lyrae stars and their average effective temperatures, we derived the relation between them from observational data. Using these relationships, we present the zero-age horizontal branch lines and corresponding evolutionary tracks in the Bailey diagrams. We first find that the trends of zero-age horizontal branch lines are consistent with the distributions of Oosterhoff I RR Lyrae stars, and there is a period shift effect in relatively metal-rich samples ( $[\text{Fe}/\text{H}] > -1$ ). Main results show that evolutionary effects are the direct cause of the Oosterhoff dichotomy. The vast majority of Oosterhoff I RR Lyrae stars are in the early stage of horizontal branch evolution, while most of the Oosterhoff II stars are near the end of the horizontal branch phase. Our Bailey diagrams can intuitively explain some Oosterhoff phenomena (e.g., long-period RR Lyrae stars in the metal-rich globular clusters NGC 6388 and NGC 6441), and also have the potential to become an important tool for in-depth study of RR Lyrae stars. Further research is needed on the Oosterhoff dichotomy to explore the formations and evolutionary processes of the Milky Way and its substructures.

*Keywords:* methods: data analysis – stars: fundamental parameters – stars: horizontal-branch – stars: pulsations – stars: variables: RR Lyrae variable

arXiv:2404.00911v2 [astro-ph.SR] 11 Nov 2024

## 1. INTRODUCTION

RR Lyrae stars are a type of short period pulsating variables widely distributed in various celestial systems within the Milky Way. They are old, small mass stars in the evolutionary stage of the horizontal branch (HB), generally believed to be over 10 billion years old. Therefore, they are one of the important probes for studying the structure and evolution of the Milky Way and neighboring galaxies (Smith 2004). Single mode RR Lyrae stars can be divided into two types: the ab-type (RRab stars) and the c-type (RRc stars). The former are dominated by the fundamental mode, while the latter are dominated by the first overtone mode with a relatively short pulsation period. In the Hertzsprung-Russell diagram (HR diagram), RR Lyrae stars also undergo evolution over time. For a metal-intermediate RR Lyrae star, it begins its evolution from the zero-age horizontal branch (ZAHB), first evolves from blue to red, then in the opposite direction, and finally turns towards the asymptotic giant branch (AGB) located in the upper right corner of the HR diagram (Bono et al. 2020). The typical lifetime of a horizontal branch star is generally 0.1 Gyr, and it may only spend a portion of its life in the Instability Strip (IS, Sandage 1957; Lee 1991; Pietrinferni et al. 2004; Le Borgne et al. 2007). In this process, the physical parameters of the stars such as luminosity, and effective temperature change with evolution. Consequently, the pulsation parameters, which are dependent on these physical parameters (e.g., period, amplitude), will also undergo changes (Di Criscienzo et al. 2004; Le Borgne et al. 2007).

Many early discovered RR Lyrae stars are located in globular clusters (GCs), and the observation and research of such stars were initially mostly focused on those in GCs (Smith 2004). One of the important discoveries was the Oosterhoff dichotomy. This phenomenon refers to significant differences in the average pulsation period distribution and the proportion of RRc stars to the total number of RR Lyrae stars in different GCs (Oosterhoff 1939). The clusters with short periods and low proportions (e.g., M3) are known as Oosterhoff type I clusters (OoI clusters), while those with long periods and high proportions (e.g., M15) are known as Oosterhoff type II clusters (OoII clusters, Smith 2004). It was later discovered that the metallicity of stars in the OoII clusters were weaker than that of stars in the OoI clusters (Arp 1955; Kinman 1959). Numerous studies have been conducted to explain the Oosterhoff phenomenon. Interested readers can refer to Smith (2004) and recent papers such as Fabrizio et al. (2021) and Zhang et al. (2023).

In the present paper, we focus on the relevant work conducted from the evolutionary perspective. Sandage (1958) suggested that OoII RR Lyrae stars are brighter than those in OoI GCs. Subsequently, Sandage et al. (1981) discovered the period shift effect based on observations of the RR Lyrae stars in GCs M3 and M15. In subsequent work, Sandage (1981a) and Sandage (1982) pointed out that this effect exists in other GCs and has a general correlation with metal abundance. In a series of Sandages works, the Oosterhoff phenomenon and period shift effect are primarily explained by an increase in luminosity with decreasing metallicity. However, the evolutionary factors have also been mentioned in Sandage (1981b). Actually, the evolutionary effect has also been noted by some other scholars. van Albada & Baker (1973) proposed that there exists a hysteresis zone in the RR Lyrae IS and used this concept to explain the proportion of RRab and RRc stars in different Oosterhoff GCs. The various evolutionary paths are crucial for supporting this perspective. The important literature that explicitly connects the Oosterhoff phenomenon to evolutionary effects should be Lee et al. (1990). Based on their calculations, they pointed out that "almost all of the RR Lyrae variables in group II clusters are highly evolved stars from the blue side of the instability strip" and "calculations for group I clusters like M3 indicate that the masses and luminosities of the RR Lyrae variables are not much different from those of the ZAHB models". The viewpoints that evolution is related to the Oosterhoff dichotomy are also supported by models and observations (Gratton et al. 1986; Caputo & de Santis 1992; Cox 1995; Clement & Shelton 1999; Lee & Carney 1999; Cacciari et al. 2005; Prudil et al. 2020; Zhang et al. 2023). With the advancement of observations, scholars have conducted numerous studies on the Oosterhoff phenomenon. However, there is still no unified consensus on the mechanisms behind this phenomenon. The evolutionary effect, as one of the explanations, has been recognized and proposed by scholars for a long time, and it is indeed not a new finding. But this viewpoint has great potential, which is why scholars have been proposing it in their work.

In recent decades, with the development of multiple photometric surveys, the number of discovered RR Lyrae stars in the Milky Way and nearby dwarf galaxies has also rapidly increased (Alcock et al. 1998; Ivezić et al. 2000; Vivas et al. 2004; Kinemuchi et al. 2006; Szczygiel & Fabrycky 2007; Soszyński et al. 2014, 2016, 2019; Clementini et al. 2019, 2023; Molnár et al. 2022). In the study of these objects, the Bailey diagrams (Bailey et al. 1919), also known as the  $P_{\text{pul}}$  - Amplitude diagram, are usually used to investigate the Oosterhoff phenomenon (Kinemuchi et al. 2006; Kunder & Chaboyer 2009; Szczygiel et al. 2009; Smith et al. 2011; Bono et al. 2020). The latest studies utilize spectral data to determine metal abundance and kinetic parameters, and combine the Bailey diagram to analyze the Oosterhoff dichotomy (Fabrizio et al. 2019, 2021; Zhang et al. 2023). The two pulsation parameters in the Bailey diagram,

pulsation period  $P_{\text{pul}}$  and amplitude, are independent of distance and reddening, and are related to the physical and evolutionary parameters of stars. The relationship between the pulsation period and these parameters is well-known (van Albada & Baker 1971). If the relationship between amplitude and these parameters can be established, we can plot the evolutionary tracks on the Bailey diagram, similar to the HR diagram, and **intuitively** compare them with the observational results. In fact, this approach has appeared in previous studies (Bono et al. 1997, 2020).

In Section 2, we utilize the data from the LAMOST low-resolution spectrum (Xiang et al. 2019) and Gaia DR3 (Gaia Collaboration 2022; Clementini et al. 2023) to establish the relationship between effective temperature ( $T_{\text{eff}}$ ) and the amplitude of the G band ( $A(G)$ ). In Section 3, we utilize the relationships between pulsation parameters and physical parameters to derive the pulsation parameters of RR Lyrae stars under various horizontal branching states, and then depict the ZAHB and evolutionary tracks in the Bailey diagram. Sections 4 and 5 are the discussion and conclusion, respectively.

## 2. RELATIONSHIP BETWEEN $T_{\text{EFF}}$ AND $A(G)$

Given the structural evolution parameters (mass,  $[\text{Fe}/\text{H}]$ ,  $T_{\text{eff}}$ , luminosity, etc.) of a horizontal branch star in the IS, its pulsation period can be obtained by using the equation provided by van Albada & Baker (1971):

$$\log P_{\text{pul}} = -1.772 - 0.68 \log \frac{M}{M_{\odot}} + 0.84 \log \frac{L}{L_{\odot}} - 3.48 \log \frac{6500}{T_{\text{eff}}}. \quad (1)$$

Therefore, all we need to do is find the correlation between the pulsation amplitude and these evolutionary parameters. Sandage (1981b) pointed out that the  $B$  band amplitude  $A(B)$  is neither a function of luminosity nor of  $[\text{Fe}/\text{H}]$ , but depends principally on  $T_{\text{eff}}$  alone. Bono et al. (1997) used a nonlinear convection model to conduct theoretical research. The studies revealed that the luminosity amplitude is closely related to the  $T_{\text{eff}}$ , and the dependence on stellar mass and metal abundance can be ignored. McNamara & Barnes (2014) also pointed out that the dependence of the light amplitude of RR Lyrae stars on temperature is independent of Oosterhoff type. They provided the equations for the relationships between the intrinsic color index  $(B - V)_0$  and the amplitudes of  $B$  and  $V$  bands, which can be used to determine interstellar reddening. Based on these literatures, we assume that the average effective temperature is the only variable in the amplitude function and use the observational results to establish the relationship between the two parameters.

The  $T_{\text{eff}}$  data come from Xiang et al. (2019), while the amplitude data we adopted are the G band amplitude  $A(G)$  provided by Gaia DR3. Xiang et al. (2019) analyzed the LAMOST low-resolution spectra, providing multiple elemental abundance data for 6 million stars, as well as corresponding atmospheric physical parameters such as  $T_{\text{eff}}$ ,  $[\text{Fe}/\text{H}]$ , and surface gravity  $\log g$ . In the present paper, we use the  $T_{\text{eff}}$  data provided in their work. In fact, the data obtained from the LAMOST spectrum have been successfully applied to RR Lyrae stars and related fields (Li et al. 2020; Liu et al. 2020, 2022; Duan et al. 2021a,b; Wang et al. 2022; Zhang et al. 2023; Cabrera Garcia et al. 2024). Using the xmatch tool from the CDS website<sup>1</sup> (Boch et al. 2012; Pineau et al. 2020), we cross-referenced the catalog provided by Xiang et al. (2019) with the Gaia DR3 RR Lyrae variable catalog (Gaia Collaboration 2022; Clementini et al. 2023) and obtained 4550 consistent results. After removing the results with  $T_{\text{eff}}$  less than 5500 K, errors of  $T_{\text{eff}}$  greater than 500 K, and  $A(G)$  greater than 1.3 mag, we finally obtained 4071 results (depicted as light gray dots in Figure 1). The observation of LAMOST can be regarded as a random sampling of the objects. Due to the asymmetry of the RRab variation curves, most of the sampling corresponds to phases with low luminosity, which corresponds to low temperature during the pulsation phase 0.5 - 0.8. It is shown in Figure 1 that most data points are concentrated in the temperature range of 6000 - 6450 K. It can also be observed that the temperature distribution range is widest with a large amplitude, and the highest temperature can exceed 8000 K. This supports the perspective of Sandage (1981b) that "amplitude is a unique function of depth of penetration into the instability strip."

We use a simple and crude method to obtain the relationship between amplitude and  $T_{\text{eff}}$ . We divide multiple regions at equal intervals between  $A(G)$  of 0.1 - 1.3 mag, and calculate the arithmetic means of the  $T_{\text{eff}}$  and  $A(G)$  for each region. The results are highlighted with black dots in Figure 1. Furthermore, we use a parabola to fit the data points and establish the relationship between  $A(G)$  and  $\log T_{\text{eff}}$  (represented by the red line in Figure 1):

$$A(G) = 0.243(.025) + 37.6(3.3) \cdot (\log T_{\text{eff}} - 3.80) - 269(92) \cdot (\log T_{\text{eff}} - 3.80)^2. \quad (2)$$

<sup>1</sup> <http://cdsxmatch.u-strasbg.fr/>

The typical exposure times for LAMOST low-resolution spectra range from tens of minutes to over an hour (Luo et al. 2019). Due to the long exposure times, the actual temperatures obtained near phase 0 should be lower than the true instantaneous maximum temperatures. It can be inferred that the average  $T_{\text{eff}}$  in Figure 1 is slightly underestimated. However, the Blazhko effect can also lead to an overestimation of  $T_{\text{eff}}$  by affecting the amplitude. The Blazhko phenomenon is mainly characterized by periodic or quasi-periodic changes in the amplitude and phase of the light curve of RR Lyrae stars, which was first noticed by Blažko (1907). It is generally believed that the existence of the Blazhko effect suppresses pulsation, leading to a decrease in pulsation amplitude (Smith 2004), but has a relatively small impact on the average temperature (Jurcsik et al. 2012). Therefore, the Blazhko effect can cause some originally high-temperature objects to appear in low-amplitude regions, leading to overestimates of the average  $T_{\text{eff}}$ .

In fact, we can use the information provided by Bono et al. (1997) and McNamara & Barnes (2014) to establish the relationship between  $A(G)$  and  $T_{\text{eff}}$ . The  $\log T_{\text{eff}}$  and  $A(B)$  of fundamental mode pulsators are provided in Tables 3 and 4 of Bono et al. (1997). Just convert the  $A(B)$  to  $A(G)$ <sup>2</sup>, and we can obtain the relationship (see green and blue pecked lines in Figure 1). Similarly, using the Equations (3, 5, 7) provided by McNamara & Barnes (2014), along with the amplitude conversion formulas for different bands, we derived the relationship between  $A(G)$  and  $T_{\text{eff}}$  (refer to the green and blue dashed lines in Figure 1). It can be seen that there are differences in the relationship trends derived from the two literatures, and our results fall exactly between their distributions. This suggests that our results are reasonable. According to Equation (2), when the minimum  $A(G)$  is 0.1 mag and the maximum  $A(G)$  is 1.3 mag, the corresponding average  $T_{\text{eff}}$  is 6260 K and 6900 K, respectively. This indicates that the width of the fundamental mode IS is about 640 K.

### 3. BAILEY DIAGRAM

After understanding the relationship between pulsation parameters and evolutionary parameters, our focus now shifts to obtaining the evolutionary parameters of HB stars. In the present paper, we use the theoretical model parameters provided by oxygen-enhanced model (Dorman 1992) and BaSTI  $\alpha$ -enhanced canonical model<sup>3</sup> (Pietrinferni et al. 2006).

The oxygen-enhanced model provided the HB evolution sequences of a large grid, in which the partial mixing has been accurately calculated during most of the evolution. It may be more suitable for stars in GCs than scaled-solar models. Dorman (1992) provided detailed ZAHB sequences at different metal abundances, and calculated the evolutionary sequences for 10-13 masses for each composition. The entire computational grid consists of 115 sequences and approximately 40,000 stellar models, each with corresponding parameters including  $[\text{Fe}/\text{H}]$ , oxygen to iron abundance  $[\text{O}/\text{Fe}]$ , helium abundance  $Y$ , post-helium-flash age, mass, luminosity,  $T_{\text{eff}}$ ,  $\log g$ , absolute magnitude in  $V$  band, color index  $B - V$ , etc. When the evolution is in the IS, Dorman (1992) also provides the mass-to-light parameter and  $\log P_{\text{pul}}$ . We are also concerned about parameters located in and near IS, but the amount of data provided by Dorman (1992) in this region is limited. Therefore, we assume that the evolutionary tracks are continuous and smooth (ignoring the possible small loops and spikes during the evolution, Sweigart & Renzini 1979), and use the evolution parameters (mass, luminosity, and  $T_{\text{eff}}$ ) in and near the IS as the fitting objects. We use linear polynomials or exponential decay as fitting formulas to obtain the Mass -  $T_{\text{eff}}$  and Luminosity -  $T_{\text{eff}}$  relationships of ZAHB and evolutionary tracks in this region. These relationships are utilized to determine the mass and luminosity, and subsequently calculate the  $P_{\text{pul}}$ . The BaSTI HB tracks offer a greater variety of stellar models, ensuring an ample number of points in the IS. They also provide the corresponding horizontal branch ages of stars. In this way, we can directly utilize the data to plot the Bailey diagrams, and evaluate the times that HB stars can stay in the IS. In this way, we can plot continuous evolutionary tracks in IS. Then, based on Equation (2) and the pulsation relation of van Albada & Baker (1971), these sequences can be plotted on the Bailey diagram.

#### 3.1. ZAHB in Bailey Diagram

In Figure 2, the solid lines display the ZAHB for different  $[\text{Fe}/\text{H}]$  on the Bailey diagram. The left panel is based on the model provided by Dorman (1992), while the right panel is based on BaSTI (Pietrinferni et al. 2006). For the case of  $Z = 0.00001$ , the minimum temperature of ZAHB star is  $\log T_{\text{eff}} = 3.94$ . Therefore, there are no ZAHB stars in the IS at this metal abundance. As a comparison, we also provide the color density map of the Gaia DR3 RRab sample. The contour lines, marked by dashed lines, display isodensity levels in increments of 100. Various colored

<sup>2</sup> In practical operation, we first convert  $A(B)$  to  $A(V)$ , and then to  $A(G)$ . The formulas used are  $A(V) = 0.00653 + 0.75896 A(B)$  and  $A(G) = 0.925 A(V) - 0.012$ . The former is obtained by linear fitting using data from Table 6 of Liu & Janes (1990), and the latter is the Equation (3) of Clementini et al. (2016).

<sup>3</sup> <http://albione.oa-teramo.inaf.it/>

blocks represent distinct numerical densities. For a single ZAHB line, the masses decrease with an increase in  $T_{\text{eff}}$  (i.e., with an increase in pulsation amplitude). However, there is a significant difference in the masses of ZAHB pulsating stars with different  $[\text{Fe}/\text{H}]$ , and the masses decrease with the increase of  $[\text{Fe}/\text{H}]$ .

The density maps in Figure 2 mainly reflect the distribution of OoI-type stars, which account for the majority of RRab stars, while most ZAHB lines in both panels follow the relationship between the period and amplitude of OoI stars. However, in the left panel, there is a slight deviation between solid lines and the highest concentration. While most of the solid lines in the right panel match the concentration. This difference should be due to the subtle differences in physical parameters between the different models. As for which situation is more realistic, it may need to be determined in conjunction with observation results. We do not cover that in this article, because it has little impact on our main results.

In the two panels of Figure 2, it can be observed that when  $[\text{Fe}/\text{H}] < -1$ , the distributions of solid lines with different  $[\text{Fe}/\text{H}]$  are not significantly different. They overlap and are even difficult to distinguish. However, when  $[\text{Fe}/\text{H}] > -1$ , as the  $[\text{Fe}/\text{H}]$  increases, the lines move towards the left of the diagram, exhibiting the period shifting phenomenon. The reason for this phenomenon may be derived from the pulsation relation. The luminosity of metal-poor ZAHB stars in the IS is higher than that of metal-rich stars. However, according to the pulsation relation of van Albada & Baker (1971), the pulsation period is not only proportional to the logarithm of luminosity, but also inversely proportional to the logarithm of mass. Therefore, for stars with  $[\text{Fe}/\text{H}] < -1$ , as  $[\text{Fe}/\text{H}]$  decreases, both their luminosities and masses increase. The impact of the two parameters is offset, and the pulsation periods are not significantly affected. However, for stars with  $[\text{Fe}/\text{H}] > -1$ , the luminosity difference between stars with different  $[\text{Fe}/\text{H}]$  increases, leading to significant differences in  $P_{\text{pul}}$ . BaSTI provides ZAHB information with  $[\text{Fe}/\text{H}] > -0.5$ , and the corresponding lines are located at the far left of the Bailey diagram, which seriously deviates from the distribution of density map. But there are indeed a small number of samples in the area where they are located, and we will introduce them in the Section 3.2 with corresponding evolutionary tracks. Finally, Figure 2 indicates that most OoI-type stars are HB stars with  $[\text{Fe}/\text{H}] < -0.5$  either on or just evolved from the ZAHB.

### 3.2. Evolutionary tracks in Bailey Diagram

#### 3.2.1. Dorman model

Similarly, we present the evolutionary tracks of HB stars with different  $[\text{Fe}/\text{H}]$  in the Bailey diagrams (Figures 3 and 4). The black dashed lines in each panel represent the ZAHB of the corresponding  $[\text{Fe}/\text{H}]$ . The solid lines with different colors represent the evolution of stars with varying masses. The gray background dots represent RRab samples from Gaia DR3. The thick gray solid lines present the division of OoI and OoII regions (Fabrizio et al. 2021), while the black solid dots represent field RRab stars with  $[\text{Fe}/\text{H}]$  similar to the values listed in individual panels (data provided by Liu et al. 2020). The red solid dots represent RRab stars in GCs (Clement et al. 2001; Clement 2017). According to the  $[\text{Fe}/\text{H}]$  of their host clusters, they are plotted in the corresponding panels. Specifically, the samples come from M15, M53, M3, M62, M4, M107, NGC 6388, and NGC 6441. The corresponding mean  $[\text{Fe}/\text{H}]$  are as follow:  $[\text{Fe}/\text{H}] = -2.3$  (Carretta et al. 2009; Vandenberg et al. 2016; Bhardwaj et al. 2021a),  $-2.06$  (Harris 2010; Boberg et al. 2016; Bhardwaj et al. 2021b),  $-1.5$  (Harris 2010; Bhardwaj et al. 2020),  $-1.3$  (Contreras et al. 2010),  $-1.1$  (Braga et al. 2015; Neeley et al. 2015),  $-0.82$  (Butler 1975),  $-0.60$  (Armandroff & Zinn 1988), and  $-0.53$  (Armandroff & Zinn 1988).

Figures 3 and 4 show rich information and details. The several evolutionary tracks on the right side of each panel represent the late stage of HB (i.e., evolving toward AGBs), with the evolution direction from the top left to the bottom right. Their positions are consistent with those of the OoII group. In addition, it can be observed that under the same  $[\text{Fe}/\text{H}]$ , the evolutionary tracks with lower masses tend to be more to the right, while the track with the highest mass tends to be more to the left, even in the Oosterhoff intermediate region (Fabrizio et al. 2019). In the OoI region, the evolutionary tracks are relatively complex. The evolutions of HB stars near the IS are as follow: first, they move slightly from ZAHB toward the red, then toward the blue (the first turning point), and finally toward the AGB with higher luminosity (the second turning point). The folding lines in the OoI region in Figure 3 and 4 represent the corresponding evolutionary turning points. Taking Panel a in Figure 3 as an example, the purple upward curve represents the first turning point, while the right purple line represents the track after the second turning point; and the yellow downward curve represents the second turning point. In addition, the evolution lines between the two turning points are also shown in the panels (the purple line on the left in Panel b, green lines on the left in Panel c and d, red line on the left in Panel e, and black line on the left in Panel f), and they evolve along the ZAHB toward the upper left, in line with the distribution of OoI stars.

From the above, we speculate that the vast majority of OoI stars are HB stars in the early stage of HB evolution (before the second turning point), while most of OoII stars are in the late stage. Some stars in the Oo Intermediate loci may be evolved targets with relatively larger masses under the same  $[\text{Fe}/\text{H}]$  conditions. From the observed results, it can be seen that there is indeed a significant difference in the  $[\text{Fe}/\text{H}]$  between OoI and OoII stars (Fabrizio et al. 2019, 2021; Zhang et al. 2023, and references therein). However, in different panels, both OoI and OoII types of samples exist simultaneously, with varying proportions of quantities. This phenomenon of coexisting at different  $[\text{Fe}/\text{H}]$  scales suggests that the main mechanism leading to the Oosterhoff dichotomy should be evolutionary effect. Of course, we do not easily deny the influence of other factors, and we will provide a brief discussion in Section 4.

Figure 4 shows the evolutionary tracks of RRab stars with relatively high  $[\text{Fe}/\text{H}]$ . They have features similar to that in Figure 3. Additionally, a rapid decrease in the sample size can be observed. But this reduction should be caused by observation effects and data processing strategies. The majority of the data in Liu et al. (2020) was obtained from the LAMOST survey, focusing on halo stars rather than targets in the Galactic disk and bulge. Additionally, in their data processing, the matching template used also imposes limitations on  $[\text{Fe}/\text{H}]$ . It can be inferred that there are more relative metal-rich RR Lyrae stars in the disk and bulge, which may have unusual formation channels (Bobrick et al. 2024). Moreover, Panels c and d in Figure 4 show that the RRab stars found in NGC 6388 and NGC 6441, which are rich in  $[\text{Fe}/\text{H}]$  and have long  $P_{\text{pul}}$  (known as the OoIII group, Pritzl et al. 2000; Catelan 2009), are stars in the late stage of HB with relatively small masses.

Based on the information provided, we summarize four cases of the evolution of RRab stars in the Bailey diagram. When the  $[\text{Fe}/\text{H}]$  is constant, HB stars with lower mass (e.g.,  $[\text{Fe}/\text{H}] = -1.66$ , Mass =  $0.62 M_{\odot}$ , Panel d of Figure 3) tend to have higher  $T_{\text{eff}}$  in the early stages of evolution, and only remain in the fundamental mode IS in the later stages. They only appear in the OoII region (Case I, see the black line in Panel d of Figure 3). The slightly higher mass stars ( $0.64 M_{\odot}$ ) are in the IS during the early stages (the first turning point) and later stages (after the second turning point), and are located in the OoI and OoII regions, respectively (Case II, see the red lines in Panel d of Figure 3). The larger mass stars ( $0.66 M_{\odot}$ ) only present in the IS during the blueward and second redward stages, and are located in the OoI and OoII regions respectively (Case III, see the green lines in Panel d of Figure 3). The stars with the highest masses ( $0.68 M_{\odot}$ ) may only be in IS during the second turning point stages, and will be in the OoI or Oo Intermediate loci (Case IV, see the blue line in Panel d of Figure 3). Caputo et al. (1978) had a similar summary. Compared to their Figure 3, we only summarized the situations for RRab stars, but provided more the examples (i.e., the Case IV).

### 3.2.2. BaSTI model

We also used the HB tracks provided by BaSTI to plot corresponding Bailey diagrams (see Figures 5, 6, and 7). Figure 5 illustrates the case of  $Z = 0.00001$ ,  $[\text{Fe}/\text{H}] = -3.62$ . Colored dotted solid lines depict the evolutionary tracks, with each point representing a stellar model. It can be seen that BaSTI provides more samples compared to Dorman (1992). In this case, all RRab stars have evolved from the blue ZAHB and are in the late stage of horizontal branch evolution. They evolve from the top left to the bottom right in the diagram, and the tracks are also located in the OoII region. The lower limit of  $[\text{Fe}/\text{H}]$  in the catalog of Liu et al. (2020) is  $-2.95$ ; therefore, there are no observed samples in Figure 5.

Figures 6 and 7 are analogous to Figures 3 and 4, illustrating the evolutionary paths of RRab stars with varying  $[\text{Fe}/\text{H}]$  in the Bailey diagrams. The meanings of the lines and points in the panels are consistent with those presented in Figures 3 and 4. Since BaSTI models are not specifically designed for the metallicity of GCs, we excluded GC RRab samples from Figures 6 and 7. In addition, for cases of  $[\text{Fe}/\text{H}] > 0$  (panels e and f of Figure 7), the catalog of Liu et al. (2020) did not have corresponding observational samples. It can be seen that Figures 6 and 7 depict the evolution of RRab stars with  $[\text{Fe}/\text{H}]$  ranging from  $-2.6$  to  $-0.5$ , and their characteristics align with those in Figures 3 and 4. Therefore, we will not repeat them.

Of interest are the cases in Figure 7 where the  $[\text{Fe}/\text{H}] > -0.5$ . Due to their ZAHB loci being located in the left side of the diagram, the tracks in the later stages of evolution are situated in both the OoI and OoII regions. This implies that these metal-rich RRab stars will be extensively spread out on the Bailey diagram. This has been demonstrated in observations. The research subjects of Fabrizio et al. (2021) contains a small number of RRab samples with  $[\text{Fe}/\text{H}] > -0.5$ , indicated by warm-colored points in their Figure 7. It can be seen that their distribution in the Bailey diagram is more extensive than that of other metal-poor samples.

The BaSTI also provides the horizontal branch age of each evolutionary node, allowing us to evaluate the time experienced by these stars in the RRab IS. Taking panel d of Figure 6 as an example ( $[\text{Fe}/\text{H}] = -1.62$ )<sup>4</sup>, the evolution of stars with masses of 0.62, 0.63, and 0.64  $M_{\odot}$  belongs to Case I. They may be in the RRab IS for approximately 4, 6, and 7 Myr, respectively. The evolution of stars with masses of 0.65 and 0.66  $M_{\odot}$  belongs to Case III. Stars with masses of 0.65  $M_{\odot}$  have evolved for 21 Myr during the blueward stage and 10 Myr during the later redward stage. The corresponding times for stars with masses of 0.66  $M_{\odot}$  are 15 and 14 Myr. Stars with masses of 0.67  $M_{\odot}$  belong to Case IV, and their time in the IS is 34 Myr. We make the following preliminary estimates: the average timescale for stars in the OoII region is 5 to 6 Myr, while the timescale for stars in the OoI region is 30 Myr. Assuming that the number of observed stars is proportional to the timescale mentioned above, we expect the ratio of OoII to OoI stars to be between 1 : 6 and 1 : 5. According to the observation results of Gaia DR3, the ratio of the two is 1 : 4.6 (31,156 : 144,194, using the thick gray solid line in Figure 3 as the segmentation criterion). If using samples from Liu et al. (2020) within this range, the ratio is 1 : 6 (a total of 995 samples, with 852 and 143 samples belonging to OoI and OoII, respectively). From this perspective, the expected ratio is essentially consistent with the observed ratio.

Pritzl et al. (2002) conducted a study on variable stars in NGC 6388 and pointed out that the bluest HB stars evolve rapidly through the IS in the article. According to their research, the timescales of the targets in the IS should be less than 400,000 years (see the tracks labeled "c" in their Figure 11, less than 2 points in the IS). We also estimated the timescales using the information provided by BaSTI. For  $Z = 0.01$ ,  $[\text{Fe}/\text{H}] = -0.60$  (similar to the metallicity of NGC 6388), the timescale for the HB stars with 0.54  $M_{\odot}$  in the OoII region is 270,000 years, which is consistent with the results of Pritzl et al. (2002). However, it should be noted that in panel b of Figure 7, the corresponding evolutionary track (black solid line) can be considered to be outside the OoII region. For the solid red line located in the center of the OoII region, the corresponding mass is 0.55  $M_{\odot}$ , and the corresponding timescale is about 6 Myr. It can be seen that for relative metal rich stars in their later stage of HB evolution, the evolutionary speed is very sensitive to the mass, and RRab stars located in the OoII region have enough time to spend within the IS. Age information can support more in-depth analysis, such as assessing the timescales in IS under different  $[\text{Fe}/\text{H}]$  conditions, the rate of period change, etc. These require more targeted analysis and are also far from the main idea of this article; therefore, they are no longer covered.

#### 4. DISCUSSIONS

As mentioned in Section 1, the practice of plotting evolutionary tracks in Bailey diagrams have already appeared in Bono et al. (1997) and Bono et al. (2020). Compared to their results, the main difference between us and them is the masses. At the same metal abundance, Bono et al. (1997) systematically used a higher mass than in our study. The same applies to the example of metal-poor samples in Bono et al. (2020). The reason for this deviation should be attributed to the theoretical model. Different models have various parameters and conditions, such as  $[\text{O}/\text{Fe}]$  and helium abundance, leading to distinct evolutionary paths. However, the overall shapes of the tracks will not be altered. For example, without considering the difference in masses, the track shapes in Figures 16 and 17 of Bono et al. (1997) are generally consistent with our results shown in Panels a and e of Figure 3. The main difference is that the ZAHB line in their Figure 17 is positioned further to the right compared to ours. In the case of  $Z = 0.0001$  ( $[\text{Fe}/\text{H}] = -2.3$ ) as reported by Bono et al. (2020), the mass used was relatively large, is 0.75  $M_{\odot}$ , and the corresponding temperature at the ZAHB was also high, is  $\log T_{\text{eff}} \sim 3.91$  (approximately 8130 K, refer to the upper-left panel of their Figure 4). The evolutionary tracks in their Bailey diagram (middle-left panel of Figure 4 in their paper) are consistent with our Case I. Bono et al. (2020) provided several examples of evolution, with only one mass condition specified for each metal abundance. Normally, the mass distribution of RR Lyrae stars in GCs should follow a certain pattern, and relying on just one evolutionary track is insufficient. Similar work has been done by Sandage (2010), but they adopted the same approach, where each GC only has one evolutionary track. As for determining which model is better, it still needs to be based on the observational results in the Bailey diagram. As introduced in Section 3, our figures are sufficient to describe the evolution of RRab stars in the Bailey diagram. The theoretical tracks align well with observational results, and can elucidate some phenomena that were previously challenging to explain. This paper also introduces a new research approach. Future scholars can establish more detailed theoretical models, construct more accurate evolutionary trajectories, and conduct more in-depth research on the specifics in the Bailey diagram,

<sup>4</sup> The reason for choosing this metal abundance is that it is closest to the mean metallicity of OoI stars,  $\langle [\text{Fe}/\text{H}] \rangle = -1.59$  (Zhang et al. 2023).

such as the HASP (Stetson et al. 2014; Fiorentino et al. 2015; Belokurov et al. 2018), and the different populations (Pietrukowicz et al. 2015, 2020).

Helium-enhanced and variation models have also been used to explain the Oosterhoff phenomenon (Jang et al. 2014). BaSTI provide ZAHB information for helium-enhanced models. Additionally, we have plotted the ZAHB lines under various  $Y$  conditions in the Bailey diagrams. When  $Y = 0.3$ , we found that these lines do indeed lie in the OoII region. This indicates that the helium enhancement effect and evolutionary effect can both contribute to RRab stars appearing in the OoII region, rather than being exclusively attributed to one or the other. We will not easily deny the former, but we can discuss which effect dominates this phenomenon. From the Bailey diagram of Gaia DR3 (gray background dots in Figure 3), it can be seen that most of the RRab stars in the Milky Way and neighboring galaxies are located in the OoI region. This region can be well described by the canonical model, indicating that the vast majority of RRab stars are not helium-enhanced. Therefore, these stars must evolve, which also implies that there will be a certain proportion of horizontal branch stars crossing the IS from the blue side. These evolved stars are located in the OoII region on the Bailey diagram. Moreover, compared to the helium-enhanced model, the evolutionary effect can naturally explain the higher average rate of period changes observed in the OoII GCs (Lee 1991; Catelan 2009). We believe that evolutionary effects still dominate. Of course, given the potential significance of helium in specific celestial systems like GCs (VandenBerg et al. 2016; Tailo et al. 2019), or the Galactic bulge (Marconi & Minniti 2018), further detailed research is necessary.

One of our works is to establish the relationship between the amplitude of RRab stars and their average  $T_{\text{eff}}$ . The primary analysis is also centered around this relationship. In fact, the relationship between pulsation amplitude and other parameters is also a topic worthy of further research. In the present paper, we simply assume that the amplitude is only related to the  $T_{\text{eff}}$ . However, some scholars suggest that other factors may have an impact or correlation on the amplitude. Lee et al. (1990) proposed that the amplitude is not solely related to temperature, but also depends on  $[\text{Fe}/\text{H}]$ . The relationships depicted in literature also indicate that the amplitude is not only correlated with the color index, but also with  $[\text{Fe}/\text{H}]$  and/or pulsation period (Caputo & de Santis 1992; Piersimoni et al. 2002; Kunder & Chaboyer 2009). The amplitude is believed to be related to the Oosterhoff type (Clement & Shelton 1999), but there is also an opposing view (McNamara & Barnes 2014). In recent years, researches on RR Lyrae stars using spectral data provided by various survey projects have mostly focused on parameters such as element abundance and radial velocity (see series of papers of Fabrizio et al. 2019 and Liu et al. 2020). However, there is a lack of relevant analysis on other physical parameters (e.g.,  $T_{\text{eff}}$ ,  $\log g$ ). Perhaps scholars can directly obtain these parameters in different pulsation phases through spectroscopy (Fossati et al. 2014; Chadid et al. 2017), and then obtain the average values. These averages can be compared with physical and pulsation parameters to identify specific statistical rules and correlations. Of course, similar work can also be done by using the photometric color index (Ngeow et al. 2017). However, eliminating the influence of interstellar extinction is a complex problem.

The viewpoint that the Oosterhoff dichotomy is caused by evolutionary effects does not necessarily negate other viewpoints and discoveries. There may be complex factors and causes behind a phenomenon. As mentioned earlier, the evolutionary effect itself involves multiple stellar physical and evolutionary parameters, including metal abundance, mass, age, etc. The differences in physical and dynamic parameters between OoI and OoII RR Lyrae stars are understandable and have been confirmed (Fabrizio et al. 2019, 2021; Iorio & Belokurov 2021; Liu et al. 2022; Zhang et al. 2023). Of course, the most relevant parameters for evolution should be the two ages: the age starting from the ZAHB (or post-helium-flash age) and the age starting from the zero-age main sequence. The former directly determines the evolutionary stage of HB stars, while the latter involves the formation and evolution of stars in specific celestial structures such as the Galactic bulge, disk, halo, GCs, and dwarf galaxies. Different evolutionary experiences of the structures have also led to various scenarios in the Bailey diagram. Broadly speaking, we concur with Zhang et al. (2023) perspective that "Oosterhoff dichotomy is the result of a combination of stellar and galactic evolution." Conversely, a deeper understanding of the Oosterhoff phenomenon may contribute to the study of the formation and evolution of galactic substructures (Fiorentino et al. 2015; Pietrukowicz et al. 2015; Belokurov et al. 2018; Prudil et al. 2019, 2020; Pietrukowicz et al. 2020; Zinn et al. 2020; Iorio & Belokurov 2021; Liu et al. 2022; Wang et al. 2022).

## 5. CONCLUSION

The mechanism behind the Oosterhoff dichotomy is an important open question in the research field of RR Lyrae stars, and the evolutionary effect is one of the frequently mentioned explanations. Noting the relationships between the pulsation parameters of pulsating stars and their evolutionary parameters, it is possible to create an "HR diagram"



with pulsation parameters as variables (Bono et al. 1997, 2020). This allows us to construct the evolutionary tracks in the Bailey diagrams. We assumed that the pulsation amplitude is a function of the average  $T_{\text{eff}}$ , and derived their relationship equation from the observed data. Based on these relationships, we convert the evolutionary parameters presented by Dorman (1992) and BaSTI into corresponding pulsation parameters, and illustrate them on the Bailey diagram (see Figures 2, 3, 4, 5, 6, 7).

Figure 2 shows that the distributions of the ZAHB RRab stars are consistent with those of OoI stars, both amplitude decreasing with the increase of  $P_{\text{pul}}$ . When  $[\text{Fe}/\text{H}] < -1$ , there is little difference in the distribution of ZAHB lines for different  $[\text{Fe}/\text{H}]$ . When  $[\text{Fe}/\text{H}] > -1$ , the difference in luminosity caused by  $[\text{Fe}/\text{H}]$  becomes significant, leading to the period shift phenomenon in the Bailey diagram (see Figure 2). The evolutionary tracks in Figures 3 - 7 suggest that the vast majority of OoI stars are HB stars in the early stage of HB evolution, while most of OoII stars are in the late stage. Some stars in the Oo Intermediate loci may be evolved targets with relatively larger masses under the same  $[\text{Fe}/\text{H}]$  conditions. These indicate that evolutionary effects are the direct cause of the Oo dichotomy. Our Bailey diagrams also intuitively solve the problem of the so-called OoIII groups with rich  $[\text{Fe}/\text{H}]$  and long  $P_{\text{pul}}$ , and have broader application prospects.

Finally, research on the Oosterhoff phenomenon will not be interrupted. Reflecting the results of HB evolution can play an important role as a clue or breakthrough point in exploring the formation and evolution process of the Milky Way and its substructures.

This work is supported by the International Cooperation Projects of the National Key R&D Program (No. 2022YFE0127300), the National Natural Science Foundation of China (Nos. 11933008, 12103084), the Natural Science Foundation of Yunnan Province (Nos. 202201AT070187, 202301AT070352, 202401AS070046), and "Yunnan Revitalization Talent Support Program" in Yunnan Province.

This research uses data from Dorman (1992), Clement et al. (2001), Pietrinferni et al. (2006), Clement (2017), Xiang et al. (2019), Liu et al. (2020), Gaia Collaboration (2022) and Clementini et al. (2023). We express our gratitude for their excellent work. Without their contributions, this paper would not have been possible to complete. This research made use of the cross-match service provided by CDS, Strasbourg. This work has made use of data from the European Space Agency (ESA) mission *Gaia* (<https://www.cosmos.esa.int/gaia>), processed by the *Gaia* Data Processing and Analysis Consortium (DPAC, <https://www.cosmos.esa.int/web/gaia/dpac/consortium>). Funding for the DPAC has been provided by national institutions, in particular the institutions participating in the *Gaia* Multilateral Agreement.

## REFERENCES

- Alcock, C., Allsman, R. A., Alves, D. R., et al. 1998, *ApJ*, 492, 190
- Armandroff, T. E., & Zinn, R. 1988, *AJ*, 96, 92
- Arp, H. C. 1955, *AJ*, 60, 317
- Bailey, S. I., Leland, E. F., Woods, I. E., & Pickering, E. C. 1919, *Annals of Harvard College Observatory*, 78, 195
- Belokurov, V., Deason, A. J., Koposov, S. E., et al. 2018, *MNRAS*, 477, 1472
- Bhardwaj, A., Rejkuba, M., de Grijs, R., et al. 2020, *AJ*, 160, 220
- Bhardwaj, A., Rejkuba, M., Sloan, G. C., Marconi, M., & Yang, S.-C. 2021a, *ApJ*, 922, 20
- Bhardwaj, A., Rejkuba, M., de Grijs, R., et al. 2021b, *ApJ*, 909, 200
- Blázquez, S. 1907, *Astronomische Nachrichten*, 175, 325
- Boberg, O. M., Friel, E. D., & Vesperini, E. 2016, *ApJ*, 824, 5
- Bobrick, A., Iorio, G., Belokurov, V., et al. 2024, *MNRAS*, 527, 12196
- Boch, T., Pineau, F., & Derriere, S. 2012, in *Astronomical Society of the Pacific Conference Series*, Vol. 461, *Astronomical Data Analysis Software and Systems XXI*, ed. P. Ballester, D. Egret, & N. P. F. Lorente, 291
- Bono, G., Caputo, F., Castellani, V., & Marconi, M. 1997, *A&AS*, 121, 327
- Bono, G., Braga, V. F., Crestani, J., et al. 2020, *ApJL*, 896, L15
- Braga, V. F., Dall'Ora, M., Bono, G., et al. 2015, *ApJ*, 799, 165
- Butler, D. 1975, *ApJ*, 200, 68
- Cabrera Garcia, J., Beers, T. C., Huang, Y., et al. 2024, *MNRAS*, 527, 8973
- Cacciari, C., Corwin, T. M., & Carney, B. W. 2005, *AJ*, 129, 267

- Caputo, F., Castellani, V., & Tornambe, A. 1978, *A&A*, 67, 107
- Caputo, F., & de Santis, R. 1992, *AJ*, 104, 253
- Carretta, E., Bragaglia, A., Gratton, R., D’Orazi, V., & Lucatello, S. 2009, *A&A*, 508, 695
- Catelan, M. 2009, *Ap&SS*, 320, 261
- Chadid, M., Sneden, C., & Preston, G. W. 2017, *ApJ*, 835, 187
- Clement, C. M. 2017, *VizieR Online Data Catalog*: Updated catalog of variable stars in globular clusters (Clement+ 2017), *VizieR On-line Data Catalog: V/150*. Originally published in: 2001AJ....122.2587C, ,
- Clement, C. M., & Shelton, I. 1999, *ApJL*, 515, L85
- Clement, C. M., Muzzin, A., Dufton, Q., et al. 2001, *AJ*, 122, 2587
- Clementini, G., Ripepi, V., Leccia, S., et al. 2016, *A&A*, 595, A133
- Clementini, G., Ripepi, V., Molinaro, R., et al. 2019, *A&A*, 622, A60
- Clementini, G., Ripepi, V., Garofalo, A., et al. 2023, *A&A*, 674, A18
- Contreras, R., Catelan, M., Smith, H. A., et al. 2010, *AJ*, 140, 1766
- Cox, A. N. 1995, in *Astronomical Society of the Pacific Conference Series*, Vol. 78, *Astrophysical Applications of Powerful New Databases*, ed. S. J. Adelman & W. L. Wiese, 243
- Di Criscienzo, M., Marconi, M., & Caputo, F. 2004, *ApJ*, 612, 1092
- Dorman, B. 1992, *ApJS*, 81, 221
- Duan, X.-W., Chen, X., Sun, W., et al. 2021a, *ApJ*, 918, 3
- Duan, X.-W., Chen, X.-D., Deng, L.-C., et al. 2021b, *ApJ*, 909, 25
- Fabrizio, M., Bono, G., Braga, V. F., et al. 2019, *ApJ*, 882, 169
- Fabrizio, M., Braga, V. F., Crestani, J., et al. 2021, *ApJ*, 919, 118
- Florentino, G., Bono, G., Monelli, M., et al. 2015, *ApJL*, 798, L12
- Fossati, L., Kolenberg, K., Shulyak, D. V., et al. 2014, *MNRAS*, 445, 4094
- Gaia Collaboration. 2022, *VizieR Online Data Catalog*: Gaia DR3 Part 4. Variability (Gaia Collaboration, 2022), *VizieR On-line Data Catalog: I/358*. Originally published in: *Astron. Astrophys.*, in prep. (2022), ,
- Gratton, R. G., Tornambe, A., & Ortolani, S. 1986, *A&A*, 169, 111
- Harris, W. E. 2010, *arXiv e-prints*, arXiv:1012.3224
- Iorio, G., & Belokurov, V. 2021, *MNRAS*, 502, 5686
- Ivezić, Ž., Goldston, J., Finlator, K., et al. 2000, *AJ*, 120, 963
- Jang, S., Lee, Y. W., Joo, S. J., & Na, C. 2014, *MNRAS*, 443, L15
- Jurcsik, J., Sódor, Á., Hajdu, G., et al. 2012, *MNRAS*, 423, 993
- Kinemuchi, K., Smith, H. A., Woźniak, P. R., McKay, T. A., & ROTSE Collaboration. 2006, *AJ*, 132, 1202
- Kinman, T. D. 1959, *MNRAS*, 119, 538
- Kunder, A., & Chaboyer, B. 2009, *AJ*, 138, 1284
- Le Borgne, J. F., Paschke, A., Vandebroere, J., et al. 2007, *A&A*, 476, 307
- Lee, J.-W., & Carney, B. W. 1999, *AJ*, 118, 1373
- Lee, Y.-W. 1991, *ApJ*, 367, 524
- Lee, Y.-W., Demarque, P., & Zinn, R. 1990, *ApJ*, 350, 155
- Li, L.-J., Qian, S.-B., Zhang, J., He, J.-J., & Zhu, L.-Y. 2020, *Research in Astronomy and Astrophysics*, 20, 094
- Liu, G., Huang, Y., Bird, S. A., et al. 2022, *MNRAS*, 517, 2787
- Liu, G. C., Huang, Y., Zhang, H. W., et al. 2020, *ApJS*, 247, 68
- Liu, T., & Janes, K. A. 1990, *ApJ*, 354, 273
- Luo, A. L., Zhao, Y. H., Zhao, G., & et al. 2019, *VizieR Online Data Catalog: LAMOST DR5 catalogs* (Luo+, 2019), *VizieR On-line Data Catalog: V/164*. Originally published in: 2019RAA.in.prep..L, ,
- Marconi, M., & Minniti, D. 2018, *ApJL*, 853, L20
- McNamara, D. H., & Barnes, J. 2014, *AJ*, 147, 31
- Molnár, L., Bódi, A., Pál, A., et al. 2022, *ApJS*, 258, 8
- Neeley, J. R., Marengo, M., Bono, G., et al. 2015, *ApJ*, 808, 11
- Ngeow, C.-C., Kanbur, S. M., Bhardwaj, A., Schreieggost, Z., & Singh, H. P. 2017, *ApJ*, 834, 160
- Oosterhoff, P. T. 1939, *The Observatory*, 62, 104
- Piersimoni, A. M., Bono, G., & Ripepi, V. 2002, *AJ*, 124, 1528
- Pietrinferni, A., Cassisi, S., Salaris, M., & Castelli, F. 2004, *ApJ*, 612, 168
- . 2006, *ApJ*, 642, 797
- Pietrukowicz, P., Kozłowski, S., Skowron, J., et al. 2015, *ApJ*, 811, 113
- Pietrukowicz, P., Udalski, A., Soszyński, I., et al. 2020, *AcA*, 70, 121
- Pineau, F.-X., Boch, T., Derrière, S., & Schaaff, A. 2020, in *Astronomical Society of the Pacific Conference Series*, Vol. 522, *Astronomical Data Analysis Software and Systems XXVII*, ed. P. Ballester, J. Ibsen, M. Solar, & K. Shortridge, 125
- Pritzl, B., Smith, H. A., Catelan, M., & Sweigart, A. V. 2000, *ApJL*, 530, L41

- Pritzl, B. J., Smith, H. A., Catelan, M., & Sweigart, A. V. 2002, *AJ*, 124, 949
- Prudil, Z., Dékány, I., Catelan, M., et al. 2019, *MNRAS*, 484, 4833
- Prudil, Z., Dékány, I., Smolec, R., et al. 2020, *A&A*, 635, A66
- Sandage, A. 1957, *ApJ*, 126, 326
- . 1958, *Ricerche Astronomiche*, 5, 41
- . 1981a, *ApJ*, 248, 161
- . 1981b, *ApJL*, 244, L23
- . 1982, *ApJ*, 252, 553
- . 2010, *ApJ*, 722, 79
- Sandage, A., Katem, B., & Sandage, M. 1981, *ApJS*, 46, 41
- Smith, H. A. 2004, *RR Lyrae Stars*
- Smith, H. A., Catelan, M., & Kuehn, C. 2011, in *RR Lyrae Stars, Metal-Poor Stars, and the Galaxy*, ed. A. McWilliam, Vol. 5, 17
- Soszyński, I., Udalski, A., Szymański, M. K., et al. 2014, *AcA*, 64, 177
- . 2016, *AcA*, 66, 131
- Soszyński, I., Udalski, A., Wrona, M., et al. 2019, *AcA*, 69, 321
- Stetson, P. B., Fiorentino, G., Bono, G., et al. 2014, *PASP*, 126, 616
- Sweigart, A. V., & Renzini, A. 1979, *A&A*, 71, 66
- Szczygieł, D. M., & Fabrycky, D. C. 2007, *MNRAS*, 377, 1263
- Szczygieł, D. M., Pojmański, G., & Pilecki, B. 2009, *AcA*, 59, 137
- Tailo, M., D'Antona, F., Caloi, V., et al. 2019, *MNRAS*, 486, 5895
- van Albada, T. S., & Baker, N. 1971, *ApJ*, 169, 311
- . 1973, *ApJ*, 185, 477
- VandenBerg, D. A., Denissenkov, P. A., & Catelan, M. 2016, *ApJ*, 827, 2
- Vivas, A. K., Zinn, R., Abad, C., et al. 2004, *AJ*, 127, 1158
- Wang, F., Zhang, H. W., Xue, X. X., et al. 2022, *MNRAS*, 513, 1958
- Xiang, M., Ting, Y.-S., Rix, H.-W., et al. 2019, *ApJS*, 245, 34
- Zhang, S., Liu, G., Huang, Y., et al. 2023, *MNRAS*, 525, 5915
- Zinn, R., Chen, X., Layden, A. C., & Casetti-Dinescu, D. I. 2020, *MNRAS*, 492, 2161

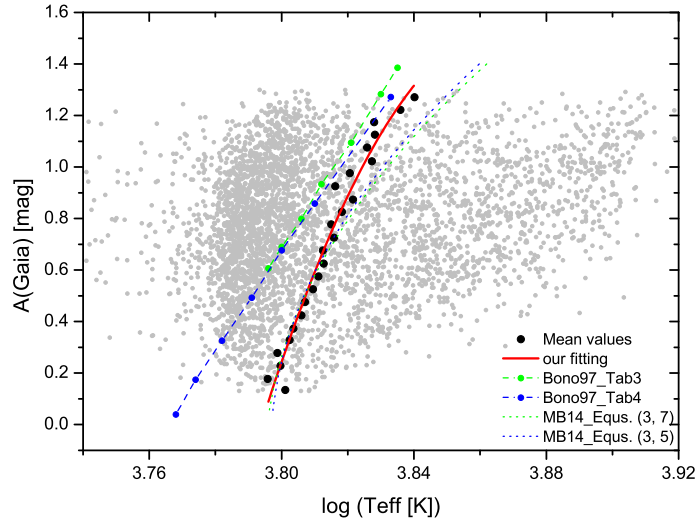


**Figure 1.**  $\log T_{\text{eff}}$  vs. Amplitude in G band. The light gray dots represent all the samples we obtained, while the black dots represent the corresponding arithmetic means. The red line represents the fit to the black dots. The pecked and dashed lines represent the relationships from Bono et al. (1997) and McNamara & Barnes (2014).  $T_{\text{eff}}$  and  $A(G)$  are obtained from Xiang et al. (2019) and Clementini et al. (2023), respectively.

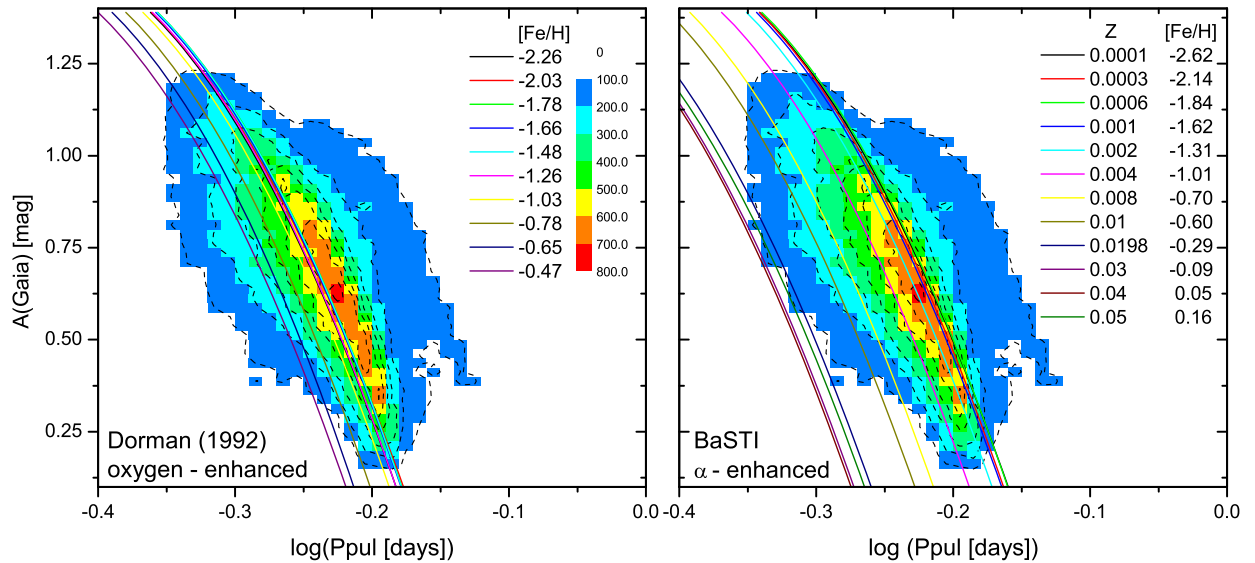


**Figure 2.** Density maps of the Bailey diagram for Gaia DR3 RRab stars. The solid lines of different colors show the ZAHB for different  $[\text{Fe}/\text{H}]$ . The dashed lines diapaly isodensity levels in increments of 100. Various colored blocks represent distinct numerical densities. Left panel: the model provided by Dorman (1992). Right panel: the model provided by BaSTI.

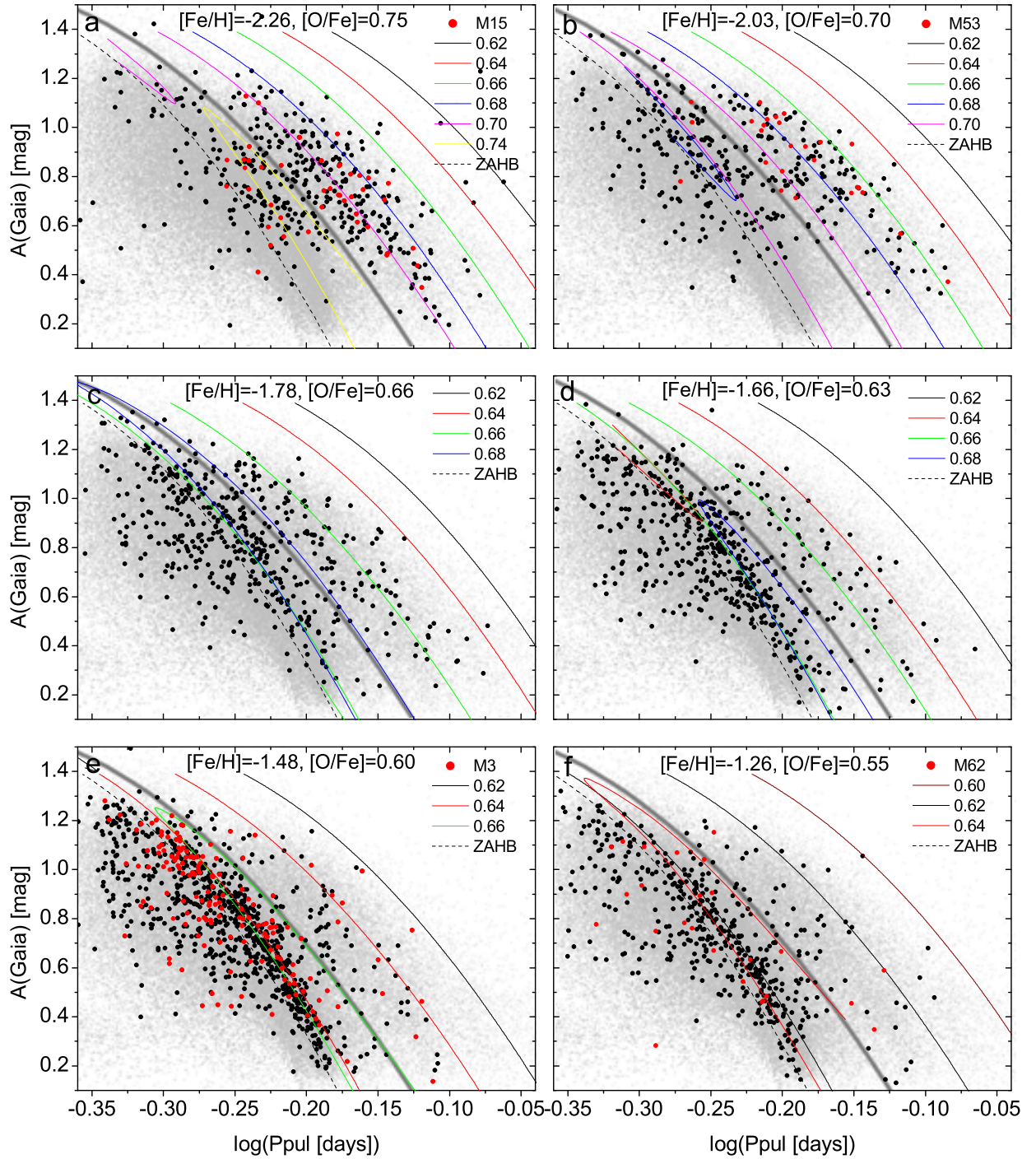


**Figure 3.** Bailey diagrams of different chemical compositions. In each panel, the gray background dots represent Gaia DR3 RRab stars, the black solid dots represent field RRab stars with corresponding  $[\text{Fe}/\text{H}]$  (Liu et al. 2020), and the red solid dots represent RRab stars in GCs (Clement et al. 2001; Clement 2017). The black dashed line in each panel refers to the ZAHB of the corresponding  $[\text{Fe}/\text{H}]$ . The solid lines represent the evolutionary tracks of stars with different masses. The thick gray solid lines present the division of OoI and OoII regions (Fabrizio et al. 2021).

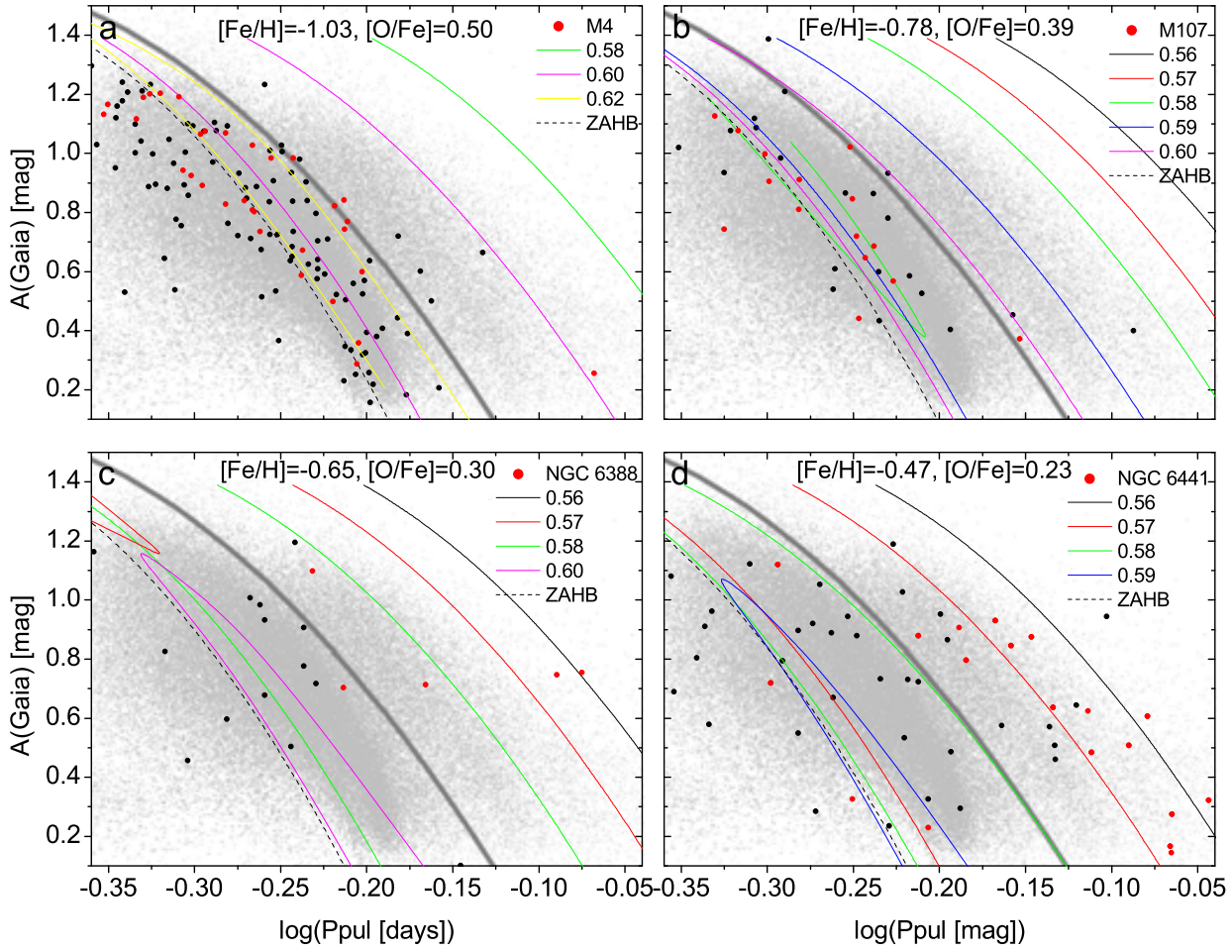


**Figure 4.** Same as Figure 3, but Bailey diagrams for those stars that are relatively metal-rich ( $[\text{Fe}/\text{H}] > -1$ ).

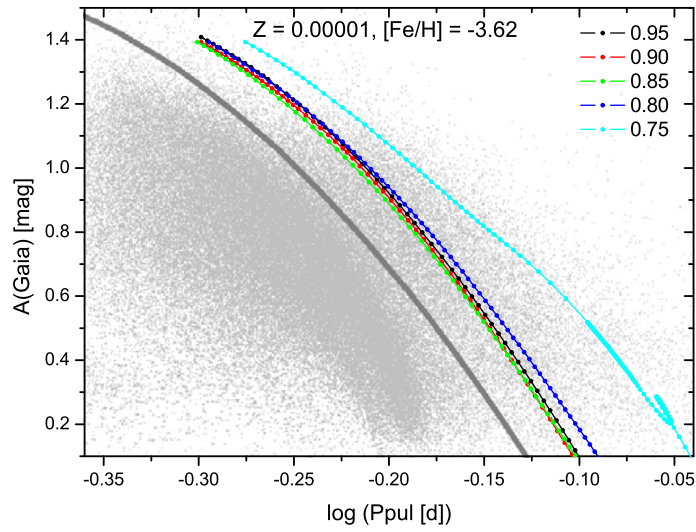


**Figure 5.** Bailey diagram for the case of  $Z = 0.00001$ ,  $[\text{Fe}/\text{H}] = -3.62$ . Colored dotted solid lines depict the evolutionary tracks, with each point representing a stellar model.

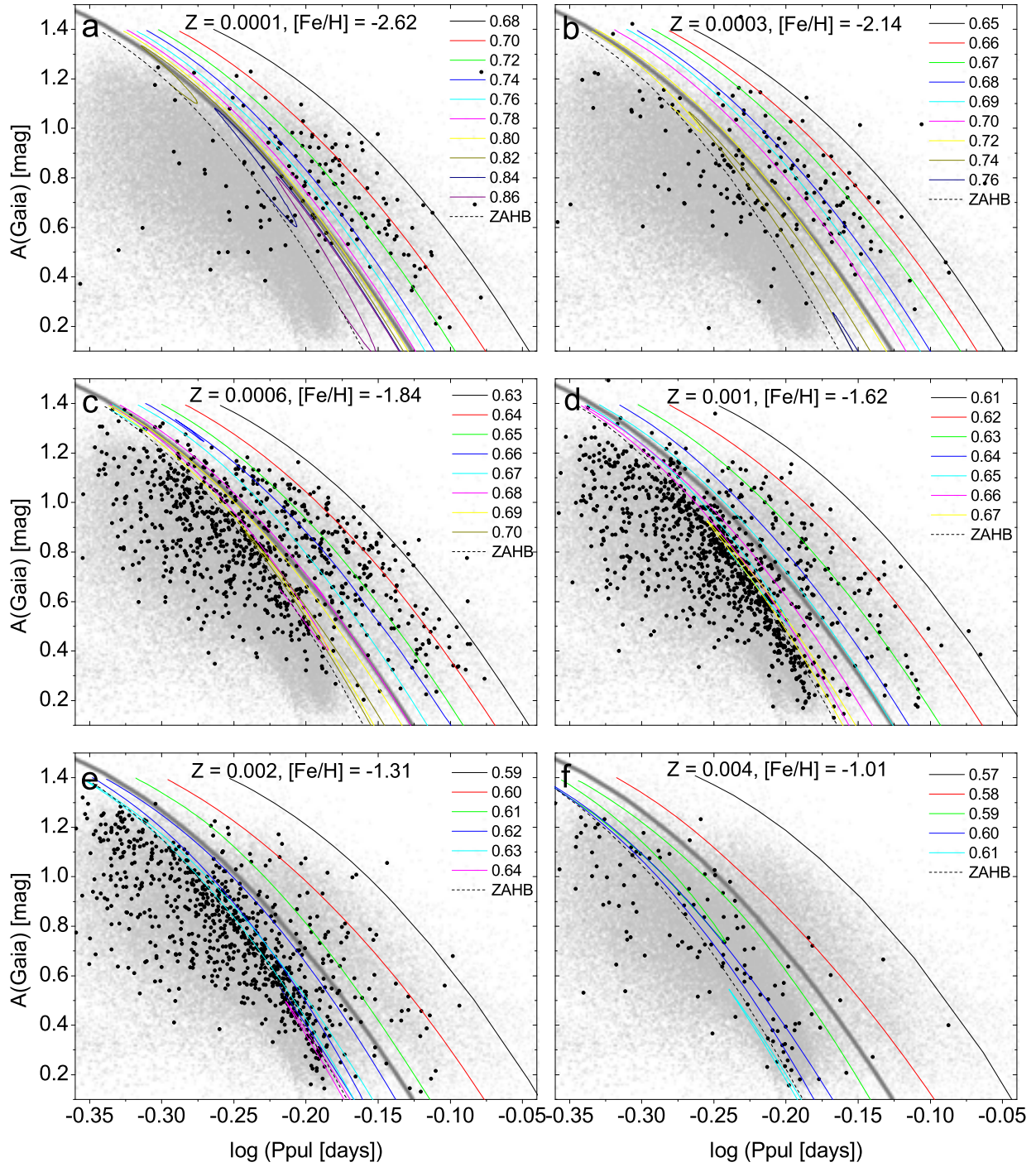
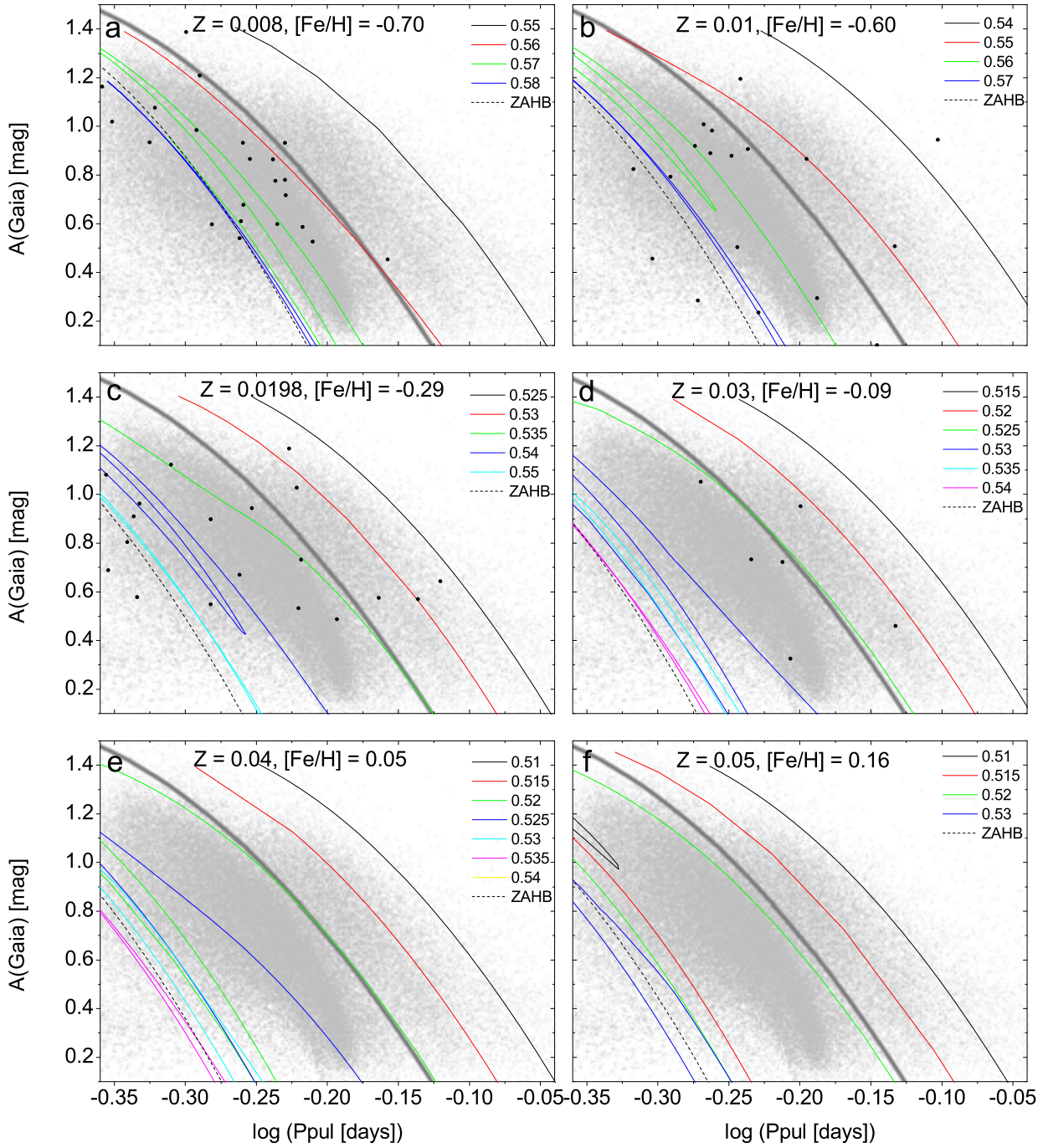


Figure 6. Same as Figure 3, but the evolutionary tracks are from BaSTI models.



**Figure 7.** Same as Figure 6, but Bailey diagrams for those stars that are relatively metal-rich ( $[\text{Fe}/\text{H}] > -1$ ).